Available online at www.sciencedirect.com
ScienceDirect
International Journal of Heat and Mass Transfer 51 (2008) 3525–3534
International Journal of HEAT and MASS TRANSFER
www.elsevier.com/locate/ijhmt

Application of CESE method to simulate non-Fourier heat conduction in finite medium with pulse surface heating

Yin Chou, Ruey-Jen Yang *

Department of Engineering Science, National Cheng Kung University, Tainan, Taiwan

Received 21 May 2007; received in revised form 10 October 2007
Available online 4 March 2008

Abstract

This study employs the space–time conservation element and solution element (CESE) method to simulate the temperature and heat flux distributions in a finite medium subject to various non-Fourier heat conduction models. The simulations consider three specific cases, namely a single phase lag (SPL) thermal wave model with a pulsed temperature condition, a SPL model with a surface heat flux input, and a dual phase lag (DPL) thermal wave model with an initial deposition of thermal energy. In every case, the thermal waves are simulated with respect to time as the thermal wave propagates through the medium with a constant velocity. In general, the simulation results are found to be in good agreement with the exact analytical solutions. Furthermore, it is shown that the CESE method yields low numerical dissipation and dispersion errors and accurately models the propagation of the wave form even in its discontinuous portions. Significantly, compared to traditional numerical schemes, the CESE method provides the ability to model the behavior of the SPL thermal wave following its reflection from the boundary surface. Further, a numerical analysis is performed to establish the CESE time step and mesh size parameters required to ensure stable solutions of the SPL and DPL thermal wave models, respectively.

Keywords: Non-Fourier heat conduction; Single phase lag (SPL) model; Dual phase lag (DPL) model; Conservation element and solution element (CESE) method

1. Introduction

In ultra-fast heat conduction systems, the orders of magnitude of time or space are extremely short, and thus the traditional Fourier conduction law with its implicit assumption of instantaneous thermal propagation is no longer applicable. As a result, special treatments are required to model the thermal transport phenomena in nano- and micro-scale systems.

Cattaneo [1] and Vernotte [2] proposed a thermal wave model with a single phase time lag, in which the temperature gradient established after a certain duration was given by

$$\vec{q} + \tau \frac{\partial \vec{q}}{\partial t} = -k\nabla T, \tag{1}$$

where τ denotes the relaxation time required for the thermal physics to include hyperbolic effect within the medium. From Eq. (1), it can be seen that when $\tau > 0$, the thermal wave propagates in the medium with a finite speed C, where $C = \sqrt{\alpha/\tau}$ (α is thermal diffusivity). However, when τ approaches zero, the thermal wave has an infinite speed and thus the single phase lag (SPL) model reduces to the traditional Fourier model.

In micro-scale conduction systems, thermal transport takes place through phonons, free electrons and photons. Hence, when the size of the physical system approaches the characteristic size of these media, it is necessary to take account of some original neglected conditions in the macro-scale, such as phonon–electron interaction, phonon scattering, and so forth. Therefore, Tzou [3] proposed the following dual phase lag (DPL) model:

$$\vec{q} + \tau_q \frac{\partial \vec{q}}{\partial t} = -k\left(\nabla T + \tau_T \frac{\partial}{\partial t}\nabla T\right), \tag{2}$$

* Corresponding author. Tel.: +886 6 2002724; fax: +886 6 2766549.
E-mail address: rjyang@mail.ncku.edu.tw (R.-J. Yang).

0017-9310/$ - see front matter © 2007 Elsevier Ltd. All rights reserved.
doi:10.1016/j.ijheatmasstransfer.2007.10.025

Nomenclature

C	speed of thermal wave
C_p	specific heat
G	amplification matrix
g	internal heat source
k	thermal conductivity
t	time
T	temperature
T_0	reference temperature
T_w	wall temperature
q	heat flux
Q	dimensionless heat flux
S	dimensionless internal heat source
x	spatial variable

Greek symbols

α	thermal conductivity
β	ratio of $(B\Delta\xi/\Delta\eta^2)$
γ	ratio of $(\Delta\xi/\Delta\eta)$
η	dimensionless space variable
λ	eigenvalue
ρ	density
τ	thermal relaxation time
θ	dimensionless temperature
ξ	dimensionless time variable

Subscripts and superscripts

m	matrix element
l	end location of film

where τ_T and τ_q re introduced to account for the finite times required for thermal equilibrium conditions to be obtained and effective collisions to take place between the electrons and the phonons, respectively.

The published literature contains many investigations into thermal wave behavior. For example, Baumeister and Hamill [4] solved the change in temperature in a semi-infinite medium under the assumption of a constant temperature boundary condition. Maurer and Thompson [5] derived an analytical solution for the non-Fourier heat conduction problem with constant heat flux boundary conditions. Özisik and Vick [6] developed analytical solutions for the hyperbolic heat conduction equation describing the wave nature of thermal energy transport in a finite slab containing a volumetric energy source and having insulated boundaries. Gembarovič and Majerni [7] calculated the temperature distribution resulting from the absorption of an instantaneous pulse of heat flux in a finite medium. Torii and Yang [8] and Lewandowska and Malinowski [9] investigated the propagation of thermal waves in thin films subjected to symmetrical heating on either side using a numerical scheme and an analytical approach, respectively. Tang and Araki [10] derived an analytical solution for the DPL model using Green's function and a finite integral transformation technique. Finally, the phase lag concept has also been employed to investigate the thermal behavior of interfacial phase compounds in metal matrix composites and thin films [11–13]. Although analytical solutions for both SPL and DPL thermal waves have been found, the solutions are limited to specific geometries and boundary conditions. Moreover, finding an exact solution invariably involves the use of a numerical technique to find the Laplace inverse transformation solution (e.g. the Riemann-sum approximation).

Numerical schemes provide a convenient means of solving thermal wave problems since they enable a variety of boundary conditions or geometric shapes to be treated using a single algorithm. Typical methods include the finite difference method and the finite element method. Gembarovic [14] solved the hyperbolic type heat conduction equation using an explicit iterative finite difference algorithm. However, the numerical solutions for the thermal wave shape deviated significantly from the exact solutions. Fan and Lu [15] employed a numerical method combining Laplace transformation and the dual reciprocity boundary element method to solve the DPL problem. However, obvious errors were observed between the numerical results and the analytical solutions. Although, many numerical solutions for thermal waves have been published, SPL thermal waves typically have a discontinuous characteristic, and hence their behavior is not easily modeled using traditional numerical schemes such as the finite difference method. Moreover, commercial software designed to simulate the temperature distribution in finite bodies is generally based on the conventional Fourier heat conduction equation, and is therefore inapplicable to the more realistic case of non-Fourier heat conduction in nano- and micro-scale systems.

The space–time conservation element and solution element (CESE) method was developed by Chang [16] in 1995 as a means of solving the Navier–Stokes and Euler equations applied in many computational fluid dynamics and aero-acoustic problems [17]. The overriding principle of the CESE method is to ensure global and local flux conservation in the space–time domain. In the CESE method, both the independent flow variables and their derivatives are treated as unknowns and are solved simultaneously. Importantly, there is no need to adjust the artificial dissipation to match the local solution properties, and hence a uniform solution accuracy is assured. These features render

the CESE method an ideal solver for wave problems characterized by discontinuous phenomena or sharp gradients, such as combustion systems, shock waves, ZND waves, and so on. Hence, this study applies the CESE method to simulate the SPL and DPL thermal waves in a finite medium subject to non-Fourier heat conduction conditions. In addition, a stability analysis is performed to establish suitable values of the CESE space and time mesh parameters when modeling SPL and DPL thermal wave systems.

2. Mathematical models

The present simulations consider three different mathematical models, as described in the sections below.

2.1. SPL model and energy equation with no internal heat source

The modified 'non-Fourier' heat flux equation and energy equation for the case of no internal heat source can be represented, respectively, as

$$q(x,t)+\tau\frac{\partial q(x,t)}{\partial t}=-k\frac{\partial T(x,t)}{\partial x}, \tag{3}$$

$$\rho C_p\frac{\partial T(x,t)}{\partial t}=-\frac{\partial q(x,t)}{\partial x}. \tag{4}$$

These coupled equations describe the temperature and heat flux distributions in the thickness (i.e. x-direction) of a film. Note that the variables τ, k and C_p denote the phase-lag time of the heat flux vector, the thermal conductivity of the medium, and the volumetric heat capacity of the medium, respectively. In dimensionless form, the temperature, heat flux and time and space variables are given, respectively, by

$$\begin{aligned}&\theta(\xi,\eta)=\frac{T(x,t)-T_0}{T_w-T_0},\quad Q(\xi,\eta)=\frac{\alpha q(x,t)}{(T_w-T_0)kC_p}\\&\xi=\frac{C^2t}{2\alpha},\quad \eta=\frac{Cx}{2\alpha}=\frac{x}{2\tau C}.\end{aligned} \tag{5}$$

where T_0 and T_w are referenced temperature and surface temperature, respectively. C is the speed of thermal wave. Using these dimensionless variables, Eqs. (3) and (4) can be rewritten as

$$\frac{\partial Q(\xi,\eta)}{\partial\xi}+\frac{\partial\theta(\xi,\eta)}{\partial\eta}=-2Q(\xi,\eta), \tag{6}$$

$$\frac{\partial\theta(\xi,\eta)}{\partial\xi}+\frac{\partial Q(\xi,\eta)}{\partial\eta}=0. \tag{7}$$

2.2. SPL model and energy equation with internal heat generation

The modified 'non-Fourier' heat flux equation and energy equation for the case where the conducting medium contains an internal heat source are given by

$$q(x,t)+\tau\frac{\partial q(x,t)}{\partial t}=-k\frac{\partial T(x,t)}{\partial x}, \tag{8}$$

$$\rho C_p\frac{\partial T(x,t)}{\partial t}=-\frac{\partial q(x,t)}{\partial x}+g(x,t). \tag{9}$$

In this particular case, the relevant dimensionless quantities are defined as follows:

$$\begin{aligned}&\theta(\xi,\eta)=\frac{T(x,t)-T_0}{g_0C_p/k},\quad Q(\xi,\eta)=\frac{\alpha q(x,t)}{g_0C^2},\\&S(\xi,\eta)=\frac{4\alpha^2q(x,t)}{g_0C^3}\quad \eta=\frac{Cx}{2\alpha},\\&\eta_l=\frac{CL}{2\alpha},\quad \xi=\frac{C^2t}{2\alpha}.\end{aligned} \tag{10}$$

In these quantities, the term g_0 denotes the internal heat flux and has the form

$$g_0=\int_{t=0}^{\infty}\int_{x=0}^{\infty}g(x,t)\,\mathrm{d}x\,\mathrm{d}t. \tag{11}$$

As shown, g_0 essentially represents the total energy released per unit area normal to the x-axis over the entire region in all time.

Based upon the dimensionless variables given in Eq. (10), the following dimensionless equations can be derived for the heat flux and temperature distributions, respectively:

$$\frac{\partial Q(\xi,\eta)}{\partial\xi}+\frac{\partial\theta(\xi,\eta)}{\partial\eta}=-2Q(\xi,\eta), \tag{12}$$

$$\frac{\partial\theta(\xi,\eta)}{\partial\xi}+\frac{\partial Q(\xi,\eta)}{\partial\eta}=\frac{1}{2}S(\xi,\eta), \tag{13}$$

2.3. DPL model

The DPL model equation and energy equation are given, respectively, by

$$q(x,t)+\tau_q\frac{\partial q(x,t)}{\partial t}=-k\left[\frac{\partial T(x,t)}{\partial x}+\tau_T\frac{\partial}{\partial t}\left(\frac{\partial T(x,t)}{\partial x}\right)\right], \tag{14}$$

$$\rho C_p\frac{\partial T(x,t)}{\partial t}=-\frac{\partial q(x,t)}{\partial x}. \tag{15}$$

The following dimensionless parameters can be introduced:

$$\begin{aligned}&\theta=\frac{T(x,t)-T_0}{T_w-T_0},\quad Q=\frac{q}{(T_w-T_0)\frac{k}{\sqrt{\alpha\tau_q}}},\quad \xi=\frac{t}{2\tau_q},\\&\eta=\frac{x}{2\sqrt{\alpha\tau_q}},\quad B=\frac{\tau_T}{2\tau_q}.\end{aligned} \tag{16}$$

Based upon these dimensionless variables, the following dimensionless equations for the heat flux and temperature distributions in the medium can be obtained:

$$\frac{\partial Q}{\partial\xi}+\frac{\partial}{\partial\eta}\left(\theta+B\frac{\partial\theta}{\partial\xi}\right)=-2Q, \tag{17}$$

$$\frac{\partial\theta}{\partial\xi}+\frac{\partial Q}{\partial\eta}=0. \tag{18}$$

3. Description of CESE scheme

Traditional numerical methods typically solve the hyperbolic type non-Fourier conduction equation for temperature using finite difference or finite element schemes. We apply the CESE scheme to treat the coupled equations including the energy equation and the thermal wave model equation (i.e. the SPL model or the DPL model) directly. Both temperature and heat flux are regarded as unknowns simultaneously. Hence, the CESE method derives the solutions at every time step for both the temperature and the heat flux.

The present analysis commences by formulating the CESE algorithm for the case of the SPL thermal wave model and energy equation with an internal heat source, i.e. case (b) above. For simplicity, Eqs. (12) and (13) can be expressed in the following matrix form:

$$\frac{\partial G_m}{\partial \xi}+\frac{\partial E_m}{\partial \eta}=F_m,\quad m=1,2 \tag{19}$$

where $G_m=\begin{bmatrix} Q \\ \theta \end{bmatrix}$, $E_m=\begin{bmatrix} \theta \\ Q \end{bmatrix}$ and $F_m=\begin{bmatrix} -2Q \\ S/2 \end{bmatrix}$. Let $x_1=\eta$ and $x_2=\xi$ be the coordinates of a two-dimensional Euclidean space E_2. Applying the Gaussian divergence theorem in E_2, the differential form of Eq. (19) can be transformed into the following integral conservation form:

$$\oint_{S(V)} \vec{h}_m\cdot \mathrm{d}\vec{s}=\int_V (F_m)\,\mathrm{d}V,\quad m=1,2 \tag{20}$$

where $\vec{h}_m=(E_m,G_m)$ and $S(V)$ is the boundary of an arbitrary space–time region V in the two-dimensional Euclidean space E_2. Essentially, the right hand side of Eq. (20) is a volume integration representing the internal heat generated over region V.

As shown in Fig. 1a, the Euclidean space E_2 is divided into an array of non-overlapping rectangular regions referred to as conservation elements (CEs). In Fig. 1b, it is shown that the CE having a top face whose midpoint coincides with mesh point (j,n) is denoted as CE(j,n). From Fig. 1c, the boundary of CE(n,j) is a subset of the union of solution element (SE) (n,j), $(n-1/2, j-1/2)$ and $(n-1/2, j+1/2)$, respectively.

For any $(\eta,\xi)\in \mathrm{SE}(j,n)$, let G_m, E_m and $\vec{h}_m$ be approximated by G_m^*, E_m^* and $\vec{h}_m^*$, respectively, with the following first-order Taylor's expansion forms:

$$\begin{aligned} G_m^*(\eta,\xi;j,n)&=(G_m)_j^n+(\eta-\eta_j)(G_{m\eta})_j^n+(\xi-\xi^n)(G_{m\xi})_j^n,\\ E_m^*(\eta,\xi;j,n)&=(E_m)_j^n+(\eta-\eta_j)(E_{m\eta})_j^n+(\xi-\xi^n)(E_{m\xi})_j^n,\\ h_m^*(\eta,\xi;j,n)&=(G_m^*(\eta,\xi;j,n),E_m^*(\eta,\xi;j,n)),\quad m=1,2. \end{aligned} \tag{21}$$

An assumption is made that a redistribution of F_m will not significantly affect the values of Q and S obtained from an averaging process involving a few neighboring conservation elements (CEs) provided that the volume integral of F_m over the CE is maintained constant. As a result, it is supposed that the internal heat source is redistributed such that there is no source present within each SE. Consequently, the following relationship can be obtained:

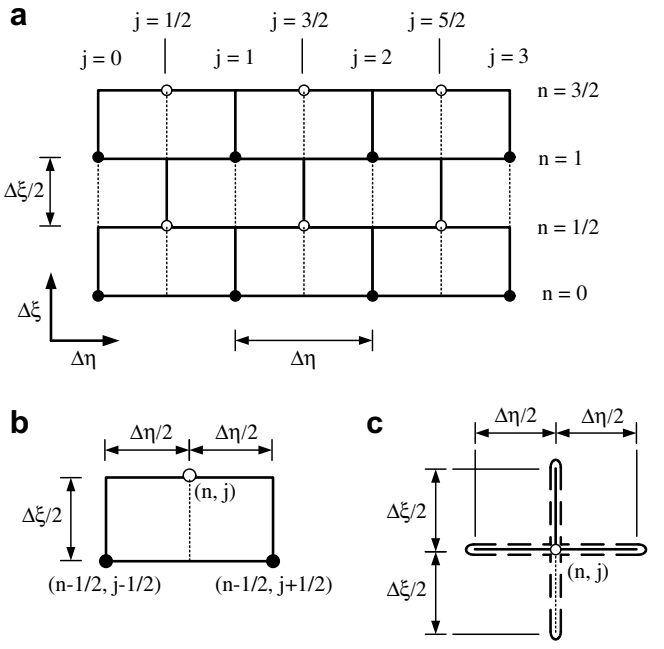

Fig. 1. Schematic illustration of space–time mesh and elements in CESE scheme: (a) staggered space–time mesh; (b) conservation element (CE) at point (n,j); (c) solution element (SE) of at point (n,j).

$$(G_{m\xi})_j^n=-(E_{m\eta})_j^n \tag{22}$$

This treatment of source term has been validated by Yu and Chang [18] in simulating ZND wave problem. From Eq. (19), it is apparent that E_m is a function of G_m. Consequently, $E_{m\eta}$ is a function of both G_m and $G_{m\eta}$. As a result, Eq. (22) implies that $G_{m\xi}$ is also a function of G_m and $G_{m\eta}$. Therefore, it can be concluded that the only independent discrete variables which need to be solved in the current marching scheme are $(G_m)_j^n$ and $(G_{m\xi})_j^n$, respectively.

The discrete approximation of Eq. (20) is given by

$$\oint_{S(\mathrm{CE}(j,n))} \vec{h}_m\cdot \mathrm{d}\vec{s}=(F_m)_j^n\times\frac{\Delta\eta\Delta\xi}{2},\quad m=1,2. \tag{23}$$

Combining Eqs. (20)–(23), it can be shown that

$$\begin{aligned} &\Delta\eta(G_m)_j^n-(F_m)_j^n\Delta\eta\frac{\Delta\xi}{2}\\ &\quad=\frac{\Delta\eta}{2}\left[(G_m)_{j-1/2}^{n-1/2}+\frac{\Delta\eta}{4}(G_{m,\eta})_{j-1/2}^{n-1/2}\right]\\ &\qquad+\frac{\Delta\xi}{2}\left[(E_m)_{j-1/2}^{n-1/2}+\frac{\Delta\xi}{4}(E_{m\xi})_{j-1/2}^{n-1/2}\right]\\ &\qquad+\frac{\Delta\eta}{2}\left[(G_m)_{j+1/2}^{n-1/2}-\frac{\Delta\eta}{4}(G_{m,\eta})_{j+1/2}^{n-1/2}\right]\\ &\qquad-\frac{\Delta\xi}{2}\left[(E_m)_{j+1/2}^{n-1/2}+\frac{\Delta\xi}{4}(E_{m\xi})_{j+1/2}^{n-1/2}\right]\quad m=1,2 \end{aligned} \tag{24}$$

Refer to Fig. 1b, the first term on the left hand side of Eq. (24) gives the flux of $\vec{h}_m$ across the top area of CE(n,j).

Meanwhile, the first and second terms on the right hand side of Eq. (24) represent the $\vec{h}_m$ fluxes across the bottom and left faces of CE(n,j), respectively, about point ($n-1/2$,$j-1/2$). Finally, the third and fourth terms denote the fluxes across the bottom and right faces of CE(n,j), respectively, about point ($n-1/2$,$j+1/2$).

To deal with the discontinuous nature of the SPL thermal wave, we adopt the damping scheme proposed in [16] to describe the special differential term $(G_{m,\eta})_j^n$, i.e.

$$(G_{m\eta})_j^n = W[(G_{m\eta-})_j^n, (G_{m\eta+})_j^n; d]. \tag{25}$$

Here, the function W be defined by

$$W[z_-, z_+; \alpha] = \frac{|z_+|^d z_- + |z_-|^d z_+}{|z_+|^d + |z_-|^d} \tag{26}$$

and has a value of zero when z_+ and z_- are zero. The coefficient d is an integer or zero. Furthermore, $(G_{m\eta\pm})_j^n$ is given by

$$(G_{m\eta\pm})_j^n = \pm\frac{(G'_m)_{j\pm1/2}^n - (G_m)_j^n}{\Delta\eta/2}. \tag{27}$$

Here $(G'_m)_j^n$ is expressed in the n-direction from point $(G_m)_j^{n-1/2}$, and thus the following form is obtained:

$$(G'_m)_{j\pm1/2}^n = (G_m)_{j\pm1/2}^{n-1/2} + \frac{\Delta\xi}{2}(G_{m\xi})_{j\pm1/2}^{n-1/2}. \tag{28}$$

Overall, Eqs. (19)–(28) describe the application of the CESE scheme to the modeling of the coupled SPL thermal wave equation and energy equation. The process of applying the CESE algorithm to compute the DPL thermal wave model is very similar to that of the SPL case. However, an important difference lies in the contents of matrix E_m. The corresponding definitions are as follows:

$$\frac{\partial G_m}{\partial\xi} + \frac{\partial E_m}{\partial\eta} = F_m, \quad m = 1, 2, \tag{29}$$

where $G_m = \begin{bmatrix} Q \\ \theta \end{bmatrix}, E_m = \begin{bmatrix} \theta + B\frac{\partial\theta}{\partial\xi} \\ Q \end{bmatrix}$ and $F_m = \begin{bmatrix} -2Q \\ 0 \end{bmatrix}$. It is observed that matrix E_m contains a derivative term of θ. However, in the current definition of the SE, the derivative term will be canceled in the first-order Taylor's expansion form, i.e. E_m^*.

4. Stability analysis

In this study, the stability of the CESE scheme is examined using the von-Neumann analysis technique with the aim being to identify suitable CESE time and space mesh size values when modeling SPL and DPL thermal waves, respectively.

4.1. SPL model

For all (j,n) belonging to the Euclidean space E_2 let

$$(G_m)_j^n = \varepsilon(n)e^{ij\phi}, \quad m = 1, 2, \ i = \sqrt{-1}, \ -\pi < \phi \leqslant \pi, \tag{30}$$

where $\varepsilon(n)$ is a 2×1 column matrix describing the disturbance at the nth time step. Substituting Eq. (30) into Eq. (24) and setting α equal to zero for a linear analysis, it can be shown that

$$\frac{\varepsilon(n)}{\varepsilon(n-1/2)} \equiv G = \begin{bmatrix} G_{11} & G_{12} \\ G_{21} & G_{22} \end{bmatrix}, \tag{31}$$

where the amplification matrix is the square of matrix G. Defining variable γ as $\gamma = \Delta\xi/\Delta\eta$, it can be shown that the elements of matrix G have the forms:

$$\begin{aligned} G_{11} &= \frac{1}{(1+\Delta\xi)}\left[\cos\left(\frac{\phi}{2}\right) + \frac{1}{4}(\gamma^2-1)(\cos\phi-1)\right], \\ G_{12} &= -i\gamma\sin\left(\frac{\phi}{2}\right)\frac{1}{(1+\Delta\xi)}, \\ G_{21} &= -i\gamma\sin\left(\frac{\phi}{2}\right), \\ G_{22} &= \cos\left(\frac{\phi}{2}\right) + \frac{1}{4}(\gamma^2-1)(\cos\phi-1). \end{aligned} \tag{32}$$

It is given by the knowledge of the eigenvalue of G which are solutions of the equation $\det[G-\lambda I]=0$. The eigenvalues of G are given by

$$\lambda = \frac{-C_1 \pm \sqrt{C_1^2 - 4C_2}}{2}. \tag{33}$$

Note that this eigenvalue has both real and imaginary parts. The coefficients C_1 and C_2 are derived from

$$\begin{aligned} C_1 &= -\frac{1}{4+\Delta\xi}(2+\Delta\xi)\left[4\cos\left(\frac{\phi}{2}\right) + (\gamma^2-1)(\cos\phi-1)\right]. \\ C_2 &= \frac{1}{16(1+\Delta\xi)}\left[4\cos\left(\frac{\phi}{2}\right) + (\gamma^2-1)(\cos\phi-1)\right]^2 \\ &\quad + \frac{\gamma^2\sin^2\phi}{1+\Delta\xi}. \end{aligned} \tag{34}$$

For a stable solution, the modulus of the amplification matrix must be bounded. In the current case, the norm of any eigenvalue of the amplification matrix must be less than 1, i.e.

$$|\lambda|^2 \leqslant 1 \tag{35}$$

where

$$\begin{aligned} |\lambda|^2 = \frac{1}{(1+\Delta\xi)}\Bigg\{&\frac{1}{8}(1-\gamma^2)^2\left[\cos\left(\frac{\phi}{2}\right)\right]^4 - (1-\gamma^2)\left[\cos\left(\frac{\phi}{2}\right)\right]^3 \\ &+\left[1-\frac{1}{4}(1-\gamma^2)\right](1-\gamma^2)\left[\cos\left(\frac{\phi}{2}\right)\right]^2 \\ &+(1-\gamma^2)\left[\cos\left(\frac{\phi}{2}\right)\right] + \left[\frac{1}{8}(1-\gamma^2)^2+\gamma^2\right]\Bigg\} \end{aligned} \tag{36}$$

The first derivative of function $|\lambda|^2$ with respect to $\cos\left(\frac{\phi}{2}\right)$ yields the extreme value of the eigenvalue. To guarantee the solution stability of the CESE scheme, it is required

that $|\lambda_{\max}|^2 \leqslant 1$. Thus, the following general limitation condition applies when the CESE scheme is employed to solve the SPL thermal wave model:

$$0 < \gamma \leqslant 1. \tag{37}$$

4.2. DPL model

The amplification matrix for the DPL model has the same form as that shown in Eq. (31) for the SPL thermal wave. Defining $\gamma = \Delta\xi/\Delta\eta$ as before, and introducing $\beta = B\frac{\Delta\xi}{\Delta\eta^2}$, the elements of G are derived as

$$\begin{aligned}
G_{11} &= \frac{1}{(1+\Delta\xi)}\left[\cos\left(\frac{\phi}{2}\right) + \left(\frac{\gamma^2}{4} - \frac{1}{4} + \beta\right)(\cos\phi - 1)\right],\\
G_{12} &= -\mathrm{i}\gamma\frac{1}{(1+\Delta\xi)}\sin\left(\frac{\phi}{2}\right),\\
G_{21} &= -\mathrm{i}\gamma\sin\left(\frac{\cos\phi - 1}{2}\right),\\
G_{22} &= \cos\left(\frac{\phi}{2}\right) + \frac{1}{4}(\gamma^2 - 1)(\cos\phi - 1).
\end{aligned} \tag{38}$$

The eigenvalues of G are again given by

$$\lambda = \frac{-C_1 \pm \sqrt{C_1^2 - 4C_2}}{2}, \tag{39}$$

in which C_1 and C_2 have the forms

$$\begin{aligned}
C_1 &= -\cos\left(\frac{\phi}{2}\right) - \frac{1}{1+\Delta\xi}\left[\cos\left(\frac{\phi}{2}\right) + \frac{1}{4}(-1 + \gamma^2 + 4\beta)\right.\\
&\quad \left.\times(\cos\phi - 1)\right] - \frac{1}{4}(\gamma^2 - 1)(\cos\phi - 1)\\
C_2 &= \frac{1}{1+\Delta\xi}\left[\cos\left(\frac{\phi}{2}\right) + \frac{1}{4}(\gamma^2 - 1)(\cos\phi - 1)\right]\\
&\quad \times\left[\cos\left(\frac{\phi}{2}\right) + \frac{1}{4}(\gamma^2 + 4\beta - 1)(\cos\phi - 1)\right] + \frac{\gamma^2\sin^2\left(\frac{\phi}{2}\right)}{1+\Delta\xi}
\end{aligned} \tag{40}$$

While too complicated for analytical stability analysis, the amplification factor given above is suitable for analysis using numerical methods, and the result will be discussed later.

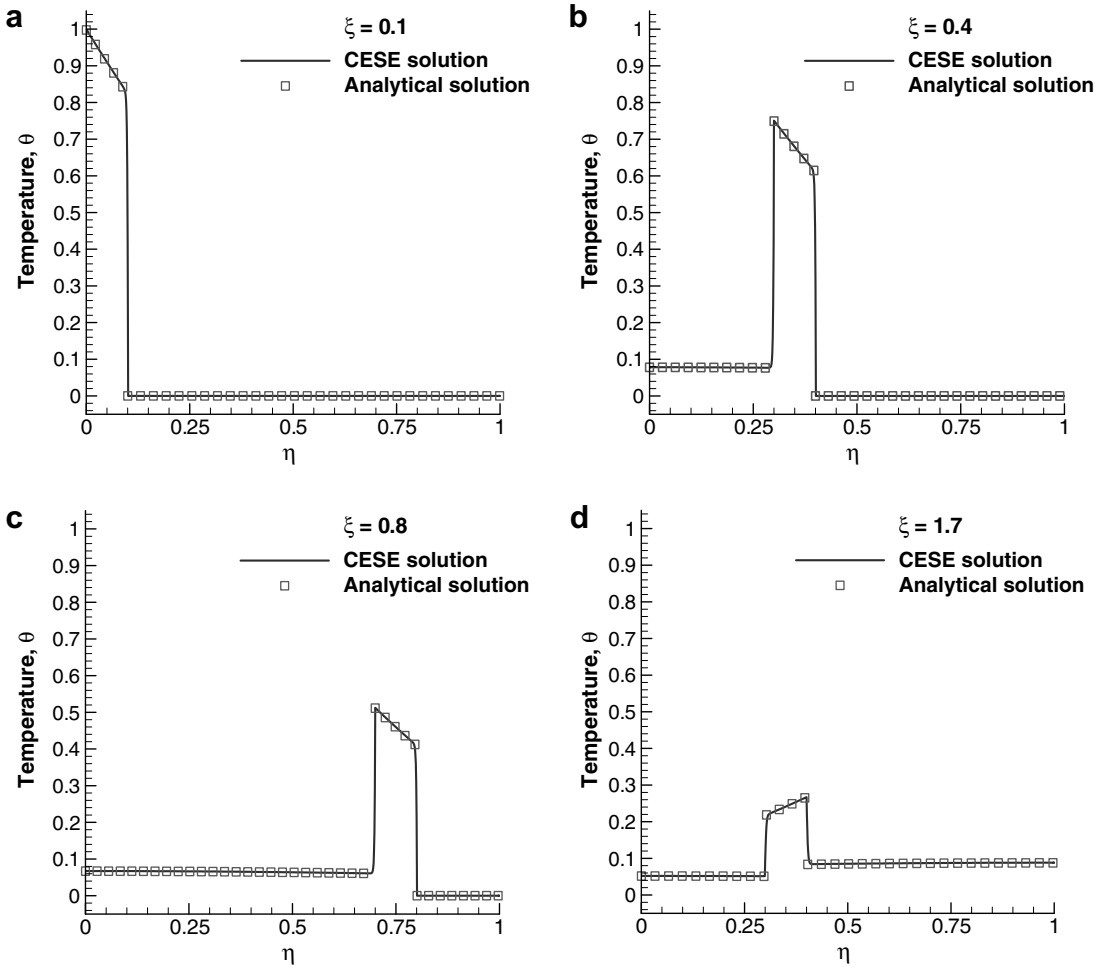

Fig. 2. Temperature distributions of SPL thermal wave computed by CESE algorithm (line) and analytical method (symbol), respectively, at dimensionless time steps of $\xi = 0.1$, 0.4, 0.8 and 1.7.

5. Results and discussion

As described below, the CESE scheme was applied to simulate a series of problems involving SPL and DPL thermal waves, respectively. In every case, the validity of the numerical results was confirmed via a comparison with the equivalent analytical solutions. Having performed the simulations, a numerical analysis was then performed to establish the CESE mesh size parameters required to ensure stable solutions of the SPL and DPL thermal wave models, respectively.

The simulations commenced by considering case (a) in Section 2 of this paper, namely an SPL thermal wave with no internal heat source. The CESE simulation results were compared with the analytical solutions presented by Gembarovič and Majerni [7]. Fig. 2a–d illustrates the temperature distribution at various elapsed times in an isotropic homogeneous finite medium with zero initial temperature, adiabatically insulated boundaries, and one surface heated by a stepwise heat pulse. The simulated film is assumed to have a uniform thickness of 1 cm and a thermal conductivity of $\alpha = 0.025\ \mathrm{cm}^2/\mathrm{s}$. Furthermore, the thermal relaxation time is specified as $\tau = 10$ s and the heat pulse is assumed to have a duration of 2 s (i.e. dimensionless duration is 0.1). Finally, the CESE parameters are assigned values of $\Delta\xi = 0.005$ and $\Delta\eta = 0.005$, respectively. Fig. 2a–c, corresponding to elapsed dimensionless times ξ of 0.1, 0.4 and 0.8, respectively, indicate that the energy of the wave front is dissipated as it propagates through the medium due to the damped effect of SPL thermal waves. The temperature discontinuities observed at the front and back of the wave, respectively, are a result of the discontinuities in the heat flux distribution function applied at the medium surface. Fig. 2d shows that the thermal wave propagates in the reverse direction following its collision with the boundary located at $\eta = 1$. Due to the essential phenomena of the hyperbolic type governing equation, the propagated wave inherits its shape from the previous time step. Moreover, the wave dissipates its energy along its propagation path due to the damped effect of the SPL model. Overall, Fig. 2a–d demonstrates that the CESE solutions for the temperature distribution are in excellent agreement with the exact analytical solutions even in the discontinuous portions of the wave form.

The second set of simulations corresponds to case (b) in Section 2, namely a SPL thermal wave in a finite medium

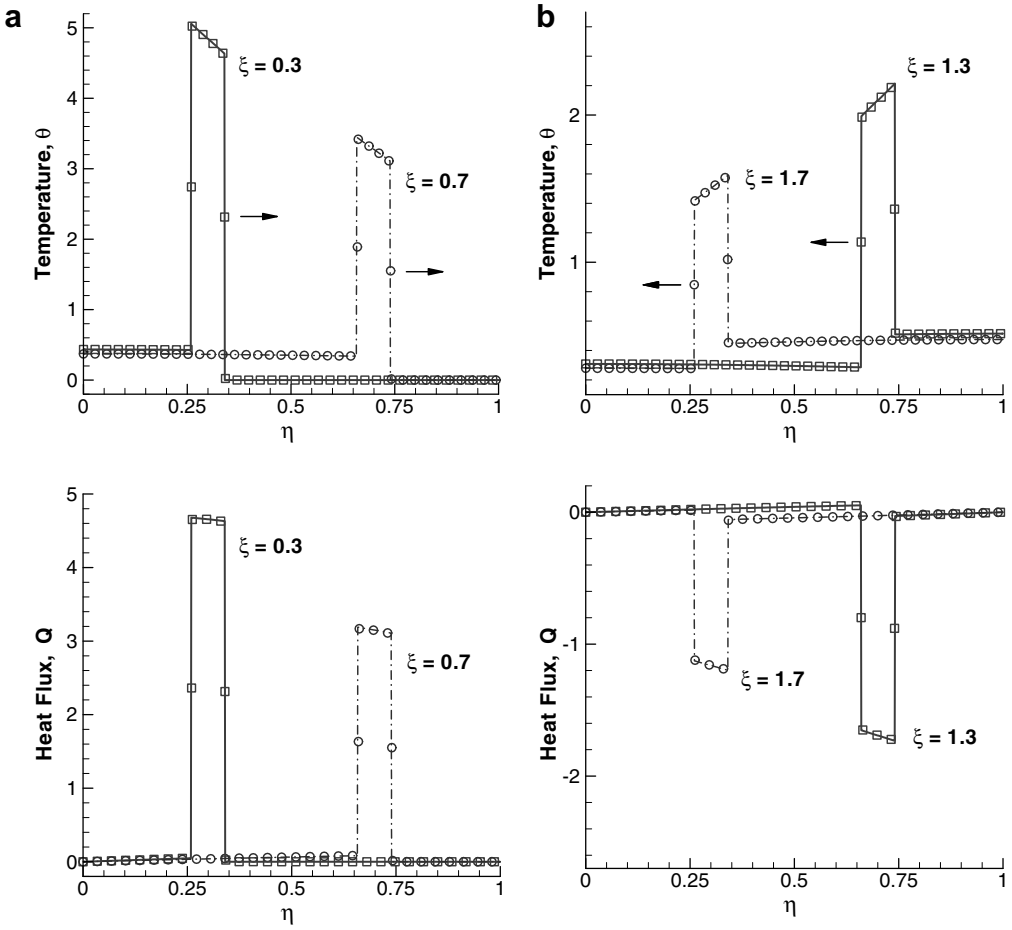

Fig. 3. Temperature and heat flux distributions of SPL thermal wave computed by CESE algorithm (line) and analytical method (symbol) at dimensionless time steps of $\xi = 0.3$, 0.7, 1.3, 1.7, 2.3 and 2.7.

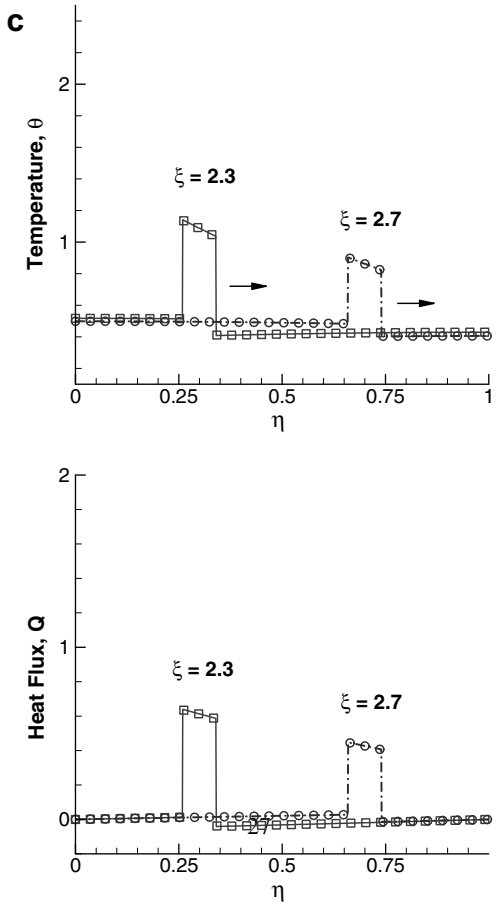

Fig. 3 (*continued*)

containing an internal heat source. In this case, the simulation results are compared with the analytical solutions presented by Özisik and Vick [6]. It is assumed that the medium (i.e. the film) has insulated boundaries and is initially in a state of thermal equilibrium. Furthermore, the position for the fixed pulse width is 0.04 from the left side of film. Finally, the CESE parameters are specified as $\Delta\xi = 0.001$ and $\Delta\eta = 0.001$, respectively. Fig. 3 illustrates the evolution of the temperature and heat flux distributions over time. Fig. 3a and b shows the temperature and heat flux distributions before and after the thermal wave reaches the medium boundary located at $\eta = 1$, respectively. Similarly, Fig. 3c shows the case where the thermal wave has been reflected from the boundary located at $\eta = 0$. Comparing the CESE solutions and the analytical results, it is evident that the CESE scheme is characterized by very low numerical dissipation and dispersion errors.

The third set of simulations relates to case (c) in Section 2 of this paper, namely a DPL thermal wave in a semi-infinite medium following an initial deposition of thermal energy over the interval $\xi = 0$ to $\xi = 0.2$. In the simulations, $\Delta\xi$ is assigned a value of 0.001 and the selected special increment $\Delta\xi$ is provided in Table 1 for different values of B (i.e. the ratio of lag time). Fig. 4a and b illustrates the temperature distribution and heat flux distribution, respectively, as a function of B. Note that values of $B = 0$ and $B = 0.5$ correspond to the particular cases of an SPL wave and thermal diffusion, respectively. The results show that as the value of B is increased, the phase lag effect suppresses the characteristic peak in the thermal wave, and the disper-

Table 1
Numerical stability experiment results: limiting value of β for CESE solution stability when applied to DPL thermal wave problem

$\Delta\xi$	B			
	0.02	0.2	0.5	1.0
1×10^{-6}	0.502	0.501	0.500	0.500
1×10^{-5}	0.506	0.502	0.501	0.500
1×10^{-4}	0.518	0.507	0.505	0.504
1×10^{-3}	0.560	0.521	0.516	0.513
1×10^{-2}	0.725	0.570	0.553	0.546

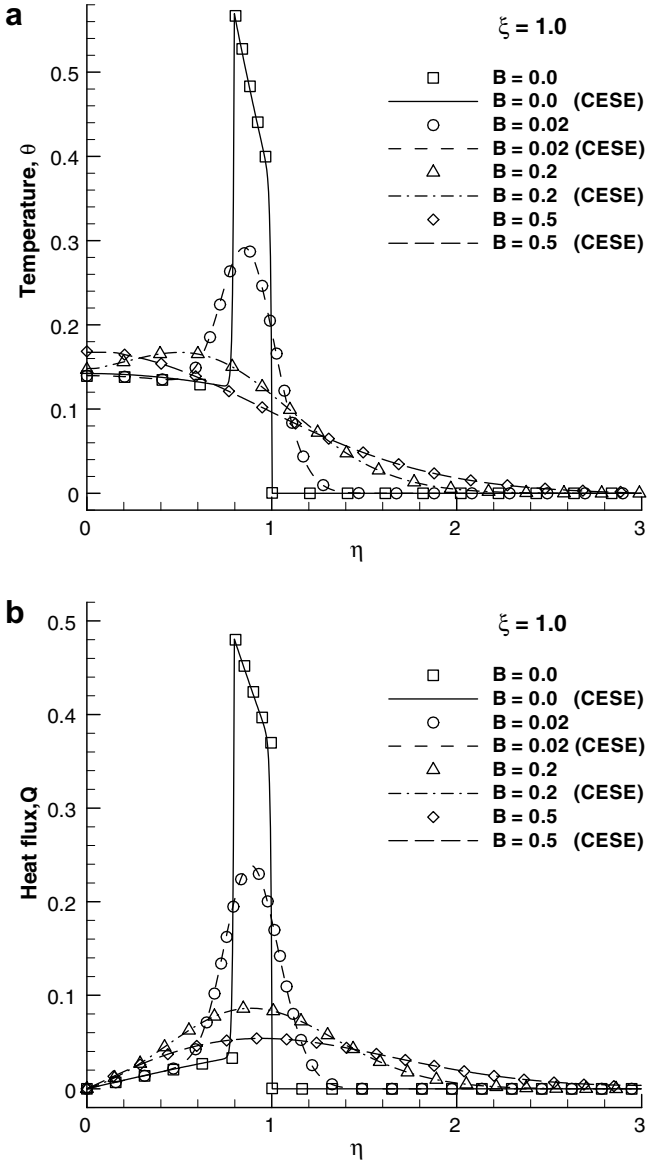

Fig. 4. (a) Temperature distribution and (b) heat flux distribution of DPL thermal wave computed by CESE algorithm (line) and analytical method (symbol) at $\xi = 0.1$ for different values of B, i.e. 0.0, 0.02, 0.2 and 0.5.

sion phenomena of the DPL model is controlled by the ratio B and reflects the effect of the two lag times (τ_T, τ_q). Furthermore, it is evident that the CESE solutions are in good agreement with the exact results.

The eigenvalues of the amplification matrix derived from Eq. (33) can be plotted using either polar coordinates or Cartesian coordinates, as shown in Fig. 5a and b, respectively. Note that in both figures, the circles labeled $R = 1$ (i.e. the radius of unit cycle) represent the demarcation line between the stable and unstable solution regimes. In Fig. 5a, it can be seen that when γ is greater than 1 (e.g. $\gamma = 1.25$), some of the values of G fall outside of the unit circle. Similarly, in Fig. 5b, some values exceed the stability limit (i.e. $|\lambda| = 1$). In other words, this particular value of γ causes the CESE solutions to become unstable. However, when γ is equal to 1, all of the values of G fall within the stable regions of the two plots since the coefficient $1/(1 + \Delta\xi)$ in Eq. (36) always smaller than 1 ($\Delta\xi > 0$). Overall, the results presented in Fig. 5 indicate that the value of the amplification matrix, G, always falls within the stable region provided that $\gamma < 1$. Consequently, it can be inferred that the parameter γ should be specified in the range $0 < \gamma \leqslant 1$ when applying the CESE scheme to model the behavior of SPL thermal waves.

Fig. 6 plots the amplification factor given in Eq. (39) for the DPL model against the value of parameter β for

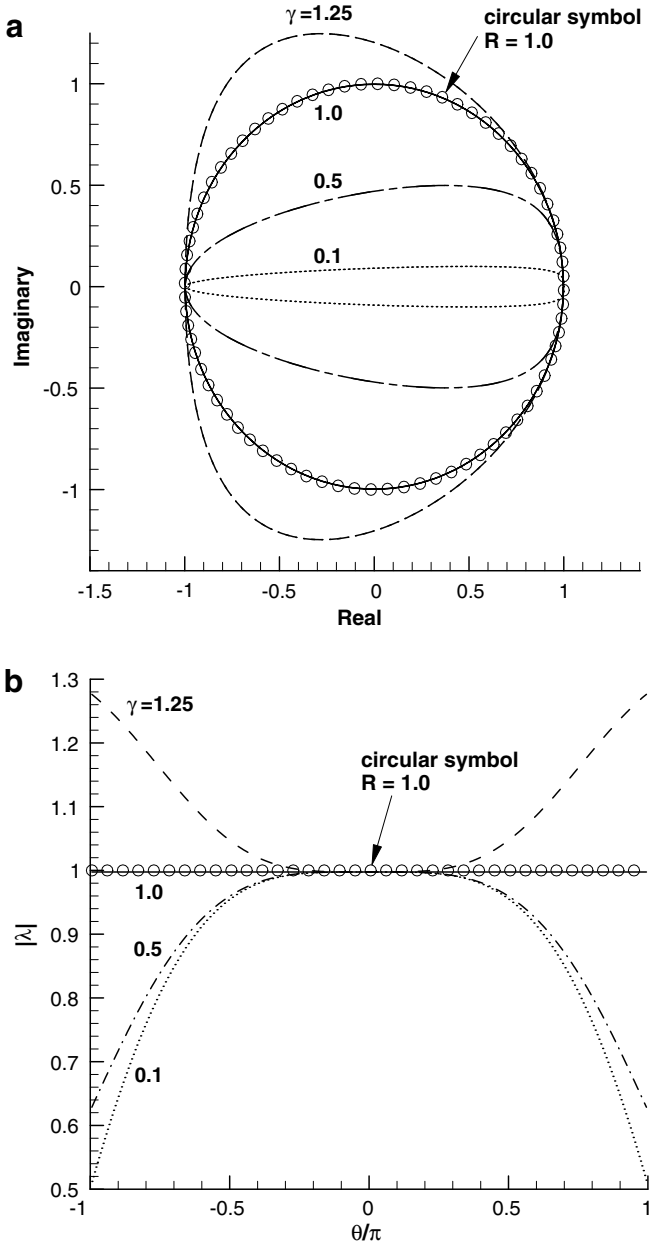

Fig. 5. Amplification factor given by eigenvalues of CESE for SPL thermal wave model expressed in terms of: (a) polar coordinates; (b) cartesian coordinates.

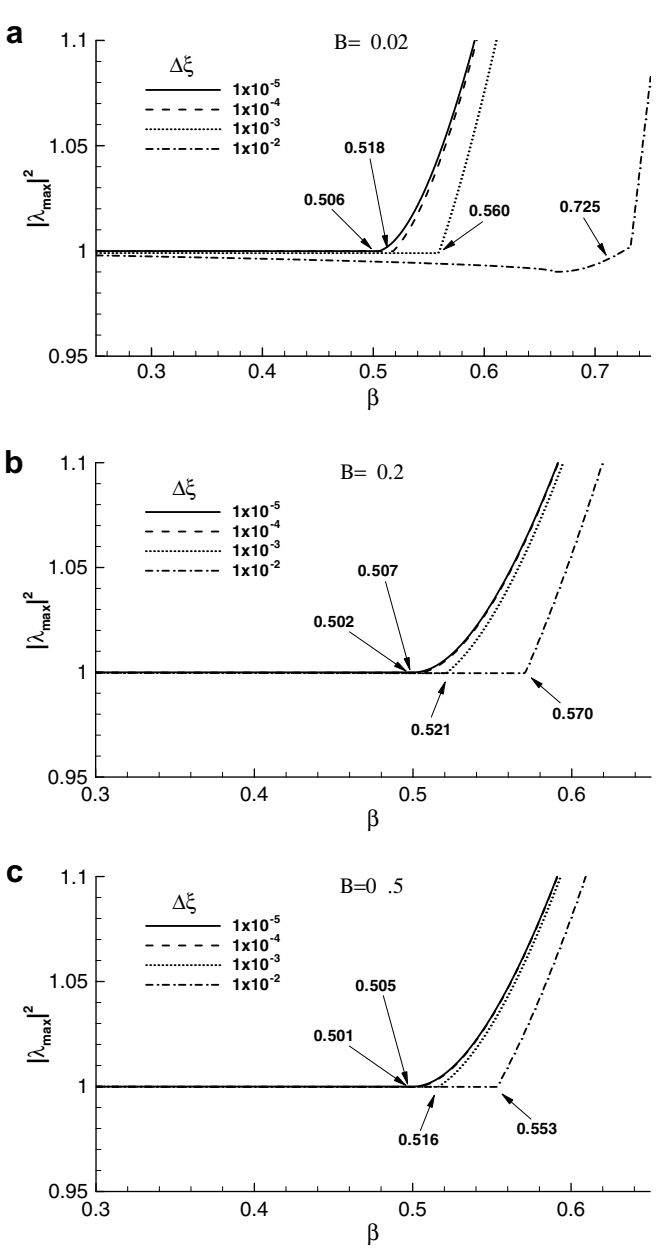

Fig. 6. Variation of $|\lambda_{max}|^2$ with β for $\Delta\xi$ equal to 1×10^{-5}, 1×10^{-4}, 1×10^{-3} and 1×10^{-2}, respectively, and different values of B, i.e. (a) $B = 0.02$, (b) $B = 0.2$, and (c) $B = 0.5$.

Table 2
Numerical stability experiment results: limiting value of $\Delta\eta$ for CESE solution stability when applied to DPL thermal wave problem

$\Delta\xi$	B			
	0.02	0.2	0.5	1.0
1×10^{-6}	2.00×10^{-4}	6.33×10^{-4}	1.00×10^{-3}	1.42×10^{-3}
1×10^{-5}	6.30×10^{-4}	2.00×10^{-3}	3.16×10^{-3}	4.47×10^{-3}
1×10^{-4}	1.97×10^{-3}	6.29×10^{-3}	9.96×10^{-3}	1.41×10^{-2}
1×10^{-3}	5.99×10^{-3}	1.96×10^{-2}	3.12×10^{-2}	4.42×10^{-2}
1×10^{-2}	1.66×10^{-2}	5.93×10^{-2}	9.51×10^{-2}	1.35×10^{-1}

various values of B, namely 0.02, 0.2 and 0.5. In each figure, the results are presented for time mesh size values of $\Delta\xi = 1 \times 10^{-2}$, 1×10^{-3}, 1×10^{-4} and 1×10^{-5}, respectively. Usage of the maximum value of $|\lambda|^2$ to determine the value of β corresponding to the edge of stability. Fig. 6a, corresponding to the case of $B = 0.02$, shows that stable CESE solutions will be obtained when β has a value of less than 0.506 and $\Delta\xi$ is equal to 1×10^{-5}. In other words, the corresponding stability criterion can be expressed as $\Delta\eta \geqslant \sqrt{(B \cdot \Delta\xi)/0.506}$. Similarly, Fig. 6b and c shows that the limiting values of β for $B = 0.2$ and $B = 0.5$ are 0.502 and 0.506, respectively (for $\Delta\xi = 1 \times 10^{-5}$). The limiting values of β and$\Delta\eta$ for various values of $\Delta\xi$ and B are summarized in Tables 1 and 2, respectively. In general, Table 1 shows that the limiting value of β reduces with decreasing $\Delta\xi$ and increasing B. Furthermore, it can be seen that when $\Delta\xi$ is reduced to 1×10^{-6} and B approaches a value of 1.0, the limiting value of β is 0.5. In other words, when applying the CESE scheme to model the behavior of DPL thermal waves, the parameters $\Delta\eta$ and $\Delta\xi$ should be specified in accordance with the condition $\Delta\eta \geqslant \sqrt{(B \cdot \Delta\xi)/0.5}$ to ensure the stability of the results. However, specifying an excessively high value of $\Delta\eta$ (e.g. $\Delta\eta = 9.51 \times 10^{-2}$) will cause serious numerical diffusion due to the corresponding loss of resolution in the grid. Furthermore, when B is equal to zero, the DPL model reduces to the SPL model, and therefore the values of $\Delta\xi$ and $\Delta\eta$ are bounded by Eq. (35).

6. Conclusion

This study has employed the space–time conservation element and solution element (CESE) scheme to model the behavior of SPL and DPL thermal waves. The simulations have considered three specific cases, namely a single phase lag (SPL) thermal wave model with a pulsed temperature condition, a SPL model with a surface heat flux input, and a dual phase lag (DPL) thermal wave model with an initial deposition of thermal energy. Furthermore, all physical behaviors are illustrated clearly in discussion section. In general, the results have shown that the CESE scheme is characterized by low numerical dissipation and dispersion errors and accurately captures the heat transfer and temperature distribution characteristics of the thermal waves even around the points of discontinuity and following reflection from the medium boundary.

This study has also performed a numerical stability analysis based on the von Neumann method to obtain some basic insights regarding an appropriate choice of space mesh size and time step size settings when applying the CESE scheme to simulate non-Fourier heat conduction problems involving SPL and DPL thermal waves. Overall, the results have shown that the ratio γ should be specified in the interval $0 < \gamma \leqslant 1$ when modeling SPL thermal waves, while $\Delta\xi$ and $\Delta\eta$ should satisfy the condition $\beta \leqslant 0.5$ when simulating DPL waves.

References

[1] C. Cattaneo, A form of heat conduction equation which eliminates the paradox of instantaneous propagation, Comput. Rendus 247 (1958) 431–433.
[2] P. Vernotte, Les paradoxes de la theorie continue de l' equation de la chaleur, Comput. Rendus 246 (1958) 3145–3155.
[3] D.Y. Tzou, Macro-to Microscale Heat Transfer: The Lagging Behavior, Taylor & Francis, Washington, DC, 1996, pp. 25–29.
[4] K.J. Baumeister, T.D. Hamill, Hyperbolic heat-conduction equation: a solution for the semi-infinite body problem, J. Heat Transfer, Ser. C 93 (1971) 126–127.
[5] M.J. Maurer, H.A. Thompson, Non-Fourier effects at high heat flux, J. Heat Transfer, Ser. C 93 (1973) 284–286.
[6] M.N. Özisik, B. Vick, Propagation and reflection of thermal waves in a finite medium, Int. J. Heat Mass Transfer 27 (1984) 1845–1854.
[7] J. Gembarovič, V. Majerni, Non-Fourier propagation of heat pulses in finite medium, Int. J. Heat Mass Transfer 31 (5) (1988) 1073–1080.
[8] S. Torii, W.J. Yang, Heat transfer mechanisms in thin film with laser heat source, Int. J. Heat Mass Transfer 48 (2005) 537–544.
[9] M. Lewandowsda, L. Malinowski, An analytical solution of the hyperbolic heat conduction equation for the case of a finite medium symmetrically heated on both sides, Int. Commun. Heat Mass Transfer 33 (2006) 61–69.
[10] D.W. Tang, N. Araki, Non-Fourier heat conduction behavior in finite mediums under pulse surface heating, Mater. Sci. Eng. A 292 (2000) 173–178.
[11] J.K. Chen, J.E. Beraun, D.Y. Tzou, A dual-phase-lag diffusion model for interfacial layer growth in metal matrix composites, J. Mater. Sci. 34 (1999) 6183–6187.
[12] J.K. Chen, J.E. Beraun, D.Y. Tzou, A dual-phase-lag diffusion model for predicting thin film growth, Semicond. Sci. Technol. 15 (2000) 235–341.
[13] J.K. Chen, J.E. Beraun, D.Y. Tzou, A dual-phase-lag diffusion model for predicting intermetallic compound layer growth in solder joins, ASME J. Electron. Packaging 123 (2001) 52–57.
[14] J. Gembarovic, Non-Fourier heat conduction modeling in a finite medium, Int. J. Thermophys. 25 (2004) 1261–1268.
[15] Q.M. Fan, W.Q. Lu, A new numerical method to simulate the non-Fourier heat conduction in a single-phase medium, Int. J. Heat Mass Transfer 45 (2002) 2815–2821.
[16] S.C. Chang, The method of space–time conservation element and solution element – A new approach for solving the Navier–Stokes and Euler equations, J. Comput. Phys. 119 (1995) 295–324.
[17] C.Y. Loh, L.S. Hultgren, S.C. Chang, Wave computation in compressible flow using space–time conservation element and solution element method, AIAA J. 39 (2001) 794–801.
[18] S.T. Yu, S.C. Chang, Treatments of stiff source terms in conservation laws by the method of space–time conservation element and solution element, AIAA 97-0435.